Capture and release of traveling intrinsic localized mode in coupled cantilever array

Masayuki Kimura[1,a)] and Takashi Hikihara[1,2,b)]
[1]*Department of Electrical Engineering, Kyoto University, Kyoto 615-8510, Japan*
[2]*Photonics and Electronics Science and Engineering Center, Kyoto University, Kyoto 615-8510, Japan*

(Received 19 September 2008; accepted 18 February 2009; published online 24 March 2009)

A method to manipulate intrinsic localized mode (ILM) is numerically discussed in a nonlinear coupled oscillator array, which is obtained by modeling a microcantilever array. Prior to the manipulation, coexistence and dynamical stability of standing ILMs are first investigated. The stability of coexisting ILMs is determined by a nonlinear coupling coefficient of the array. In addition, the global phase structure, which dominates traveling ILMs, is also changed with the stability. It makes possible to manipulate a traveling ILM by adjusting the nonlinear coupling coefficient. The capture and release manipulation of the traveling ILM is shown numerically. © *2009 American Institute of Physics*. [DOI: 10.1063/1.3097068]

Energy localization is very often observed in spatially extended system. Even in a homogeneous coupled oscillator, a localized excitation is caused by discreteness and nonlinearity. The localized excitation is intrinsic localized mode, which is also called discrete breather, first found by Sievers and Takeno. By various theoretical and numerical studies, properties of intrinsic localized mode have been revealed. In addition, experimental studies recently appear to confirm the properties. Intrinsic localized mode is observed in electronic circuit ladders, optical wave guides, and micromechanical oscillator arrays. It has been suggested that intrinsic localized mode can be utilized for applications to practical engineering. A new application using localized oscillations should include appropriate control methods. The basis of such control methods is the manipulation of the intrinsic localized mode. We discuss how to manipulate a localized excitation.

I. INTRODUCTION

Intrinsic localized mode (ILM) is a spatially localized and temporally periodic solution in nonlinear discrete systems. ILM was analytically discovered by Sievers and Takeno in 1988.[1] They identified the ILM in the Fermi–Pasta–Ulam lattice.[2] After the discovery, ILM in nonlinear discrete systems has attracted many researchers. That is, the existence, the stability, the movability, and other properties of ILM have been investigated theoretically and numerically for a variety of physical systems.[3] Experimental studies have recently appeared.[4] ILM is experimentally generated or observed in various systems, for instance, Josephson-junction array,[5,6] optic wave guides,[7,8] photonic crystals,[9] micromechanical oscillators,[10] mixed-valence transition metal complexes,[11,12] antiferromagnets,[13] and electronic circuits.[14] These experiments suggest the phenomenological universality of ILM and the possible application phase. Studies have indeed appeared toward potential applications in both fundamental science and practical engineering.[4]

Sato and co-workers[10,15] showed the existence of intrinsic localized modes in microcantilever arrays. By externally exciting the array, standing ILMs fixed at a site of the array were observed. It was also identified that a localized excitation wandered in the array. The wandering excitation is called traveling ILM in this paper. In the experiments, the traveling ILM was finally captured at a site and survived as a standing ILM. Therefore, standing ILMs can be generated by capturing a traveling ILM at a site. Recently, Sato and co-workers[16,17] manipulated the position of ILM using a localized impurity. A standing ILM was attracted or repulsed by the impurity. The attractive and repulsive manipulations allow shifting the position of standing ILM without decaying the concentrated energy of ILM. The observations and the manipulations show that the stable standing ILM exists and it can be relocated even in a micrometer scale device such as the microcantilever array. That is, ILM can be applicable to both micro- and nanoengineering.

A microcantilever array can be modeled by a simple coupled nonlinear differential equation[17] with nonlinearity in both on-site and intersite terms. It has been shown that several ILMs coexist in the array, and the dynamical stability of these coexisting ILMs depends on the ratio of nonlinearity in on-site and intersite terms.[18] In addition to that, the bifurcation structure concerning the stability change has been investigated. To study the mechanism of the transition of traveling ILMs, it is also necessary to analyze on how a traveling ILM behaves in phase space.

The relationship between traveling waves and the global phase structure was discussed in a coupled magnetoelastic beam system, which is modeled as a simple coupled nonlinear differential equation having the same form as of a microcantilever array.[19–21] They suggested that the transition of traveling wave is governed by the phase structure in the vicinity of coexisting standing waves. Standing ILMs in the

a)Electronic mail: kimura@dove.kuee.kyoto-u.ac.jp.
b)Electronic mail: hikihara@kuee.kyoto-u.ac.jp.

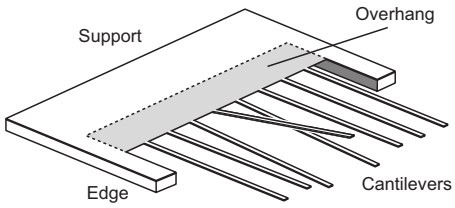

FIG. 1. Schematic configuration of coupled cantilever array. The array has eight cantilevers arranged in one dimension. Both ends of the array are fixed by support.

microcantilever array are assumed to have similar dynamics as the standing wave solutions. That is, it is conjectured that a traveling dynamics of ILM is governed by the phase structure around standing ILMs.

The purpose of this study is to propose a new method for manipulation of ILMs in the coupled oscillators which has nonlinearities in both on-site and intersite terms. Both the traveling ILMs and the corresponding global phase structure are numerically investigated. Then a manipulation method is discussed based on the phase structure. The manipulation can be achieved by adjusting the coefficient of the nonlinear intersite term.

For the research presented in this paper, a microcantilever array that exhibited ILMs was chosen as coupled oscillators. Parameter settings for the coupled oscillators are discussed in Sec. II. In Sec. III, the coexistence and the stability are investigated with respect to various values of the nonlinear coupling coefficient. The relationship between a traveling ILM and the global phase structure is discussed in Sec. IV. Finally manipulations of an ILM are shown in Sec. V.

II. COUPLED CANTILEVER ARRAY

A microcantilever array fabricated by Sato *et al.* is treated as a coupled oscillator array in this paper. A schematic configuration of the cantilever array is shown in Fig. 1. Eight cantilevers are arranged with equal intervals in one dimension. Adjacent cantilevers are coupled by the overhang. The size of the array is determined as in Ref. 15. A cantilever has a length of 50 μm, a width of 15 μm, and a thickness of 300 nm. All cantilevers are arranged with a pitch of 40 μm. Overhang region has a length of 60 μm and a thickness of 300 nm.

The vibration of a single cantilever is described by partial differential equation. Since the cantilever is thin, Euler–Bernoulli beam theory can be applied to the cantilever. The theory gives us resonant frequencies of the cantilever. The lowest frequency corresponds to the first mode oscillation of the cantilever. Because the microcantilever array was excited near the lowest frequency,[15] the motion of the tip of cantilever is modeled by a simple spring-mass system, which has the same resonant frequency as the original cantilever.

On the basis of the theoretical[22–24] and the experimental analyses,[17] the spring has cubic nonlinearity in the restoring force. Therefore the single cantilever is represented by a spring-mass system having cubic nonlinearity in the spring. The overhang is modeled the same way.[17] The difference in displacement of neighboring cantilevers causes the deformation of the overhang region. The restoring force caused by the deformation of the overhang has cubic nonlinearity.[17] Therefore the microcantilever array is expressed by

$$\ddot{u}_n = -\alpha_1 u_n - \alpha_2\{(u_n - u_{n-1}) + (u_n - u_{n+1})\} - \beta_1 u_n^3 - \beta_2\{(u_n - u_{n-1})^3 + (u_n - u_{n+1})^3\}, \quad (1)$$

where the displacement of the tip of nth cantilever is depicted by u_n. The first and third terms represent the restoring force caused by bending each cantilever. The coupling force is depicted by the second and forth terms.

Equation (1) is nondimensional and is obtained by scaling time and length. The time scaling is applied to the original differential equation so that α_1 is unity. The coefficient of nonlinear on-site restoring force is set to 0.01 by the scaling in length. Values of 5.38 μs and 2.67 μm are chosen as units of time and length. The linear coupling force was experimentally estimated to be one-tenth of the on-site restoring force.[15] Thus we assumed that the linear and nonlinear coupling coefficients are one-tenth of the corresponding coefficient to on-site force, i.e., $\alpha_2=0.1$ and $\beta_2=0.001$.

The nondimensional form shows that a microcantilever array is characterized by coupling coefficients in the nondimensional differential equation. These coupling coefficients can be thought of as the ratio of on-site and intersite coefficients. Because the coefficients in Eq. (1) depend on the length and the thickness of the cantilever and the overhang, the pitch of arranged cantilevers, Young's modulus, and the second moment of area,[17] the ratio can be selected in the design of a microcantilever array. In particular, it has been reported that the ratio in nonlinear on-site and intersite coefficients governs the stability of ILM.[18] The behavior of traveling ILM can be changed with the nonlinearity ratio. Thus, properties of standing ILMs and traveling ILMs are investigated numerically for various values of the nonlinearity ratio in this paper.

III. STANDING ILMs AND ITS STABILITY

A. Numerical techniques

In order to obtain a time-periodic solution, the shooting method using Newton–Raphson method is applied.[25] Since ILMs for Eq. (1) are time-periodic solutions, they can be found by the shooting method. Equation (1) is integrated with an initial guess over a given period T. The initial guess is estimated by a computational technique using anticontinuous limit.[26] If the initial guess is close enough to an ILM solution for Eq. (1), the ILM is obtained with the given period T.

The total energy of the ILM, $\mathcal{H}$, is a function of the period of the ILM, $\mathcal{H}=\mathcal{H}(T)$. The function, $\mathcal{H}(T)$, is a single valued function when the ILM is sufficiently localized. The total energy monotonically increases with decreasing the period T of ILM because Eq. (1) has hard nonlinearity for the on-site and the intersite restoring forces. Therefore, an ILM on certain energy surface, which is defined by a given total energy, can easily be found by Newton–Raphson method. The total energy is set at 250.

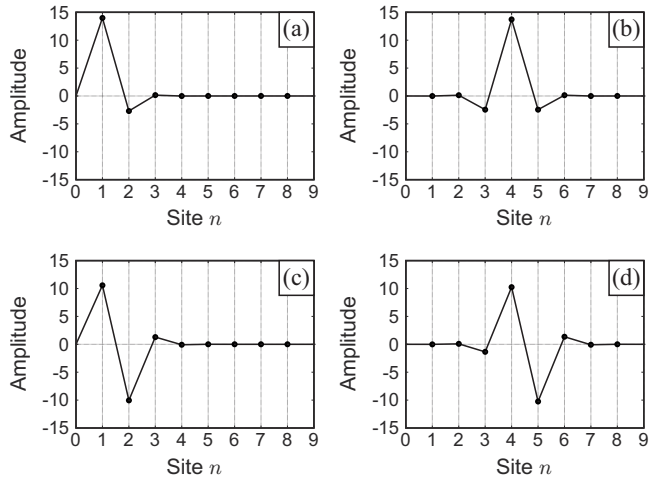

FIG. 2. Coexisting ILMs at $\beta_2=0.001$, $\mathcal{H}=250$: (a) ST1, (b) ST4, (c) P1-2, and (d) P4-5. The sixth order symplectic integrator is applied for the integration.

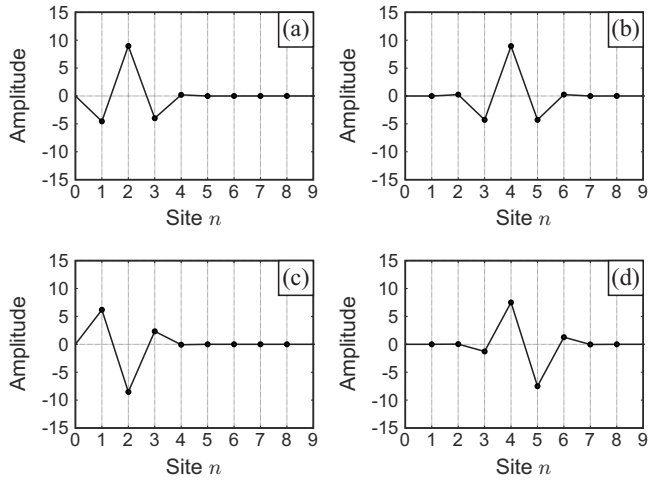

FIG. 3. Coexisting ILMs at $\beta_2=0.01$, $\mathcal{H}=250$: (a) ST2, (b) ST4, (c) P1-2, and (d) P4-5.

A periodic solution can be treated as a fixed point on a hyper surface. The dynamics around the fixed point is represented by the Poincaré map defined on the surface. Here we introduce a hyperplane

$$\Sigma_p = \{(\mathbf{u},\dot{\mathbf{u}}) \in \mathbb{R}^{16} | u_p \rangle 0,\ \dot{u}_p = 0\}, \tag{2}$$

where p is the index of cantilever and is set at 4 without loss of generality. An ILM solution corresponds to a fixed point $\mathbf{x}^* \in \Sigma_p$ for the Poincaré map $\mathcal{P}:\Sigma_p \to \Sigma_p$. Then the stability of the ILM is equivalent to the stability of the fixed point. The linearization of the map $\mathcal{P}$ leads to the linear map at the fixed point $\mathbf{x}^*$:

$$\xi_{k+1} = \mathcal{DP}(\mathbf{x}^*)\xi_{\mathbf{k}}, \tag{3}$$

where ξ depicts a variation. The matrix $\mathcal{DP}(\mathbf{x}^*)$ has 15 different eigenvalues which correspond to Floquet multipliers. An ILM is determined to be unstable if one of the 15 eigenvalues is outside unit circle on complex plane. Because Eq. (1) is a Hamiltonian system, an ILM is not determined to be unstable if and only if the all of eigenvalues are on a unit circle.

B. Coexistence of ILM

Equation (1) has several coexisting ILMs. In this paper, these ILMs are roughly classified into ST and P modes only by the symmetry of amplitude distribution. ST modes have odd-symmetric amplitude distributions. Since the locus of ST mode is at a site, its value becomes an integer. P modes have even-symmetric amplitude distribution. Then X_{ILM} takes half-integer. Coexisting ILMs in the cantilever array can be distinguished by the index number of oscillators having large amplitude because the translational symmetry is broken by the fixed ends of array. In this paper, a ST mode standing at mth site is called STm. A P mode is depicted P$m-m'$, where $m'=m+1$, because the P mode has even symmetric in amplitude distribution. The locus of the P mode is found at $m+1/2$.

Coexisting ILMs at $\beta_2=0.001$ are shown in Fig. 2. The ends of array correspond to $n=0$ and 9. Figure 2(a) shows a ST mode standing at $n=1$. The ST mode is labeled as ST1. Other ILMs shown in Figs. 2(b)–2(d) are labeled as ST4, P1-2, and P4-5, respectively. Eight ST modes and seven P modes are found at $\beta_2=0.001$. Figure 3 shows coexisting ILMs at $\beta_2=0.01$, which is ten times larger than the former case. In this array, six ST modes and seven P modes coexist. ST2, ST4, P1-2, and P4-5 are shown in Figs. 3(a)–3(d), respectively. ST1 was not found for this array by using our method. In addition, the symmetry of P1-2 is obviously broken, that is, the amplitude of the first and second oscillators are different. The disappearance of ST1 and the symmetry breaking of P1-2 are due to an increase in the influence of the fixed boundary with β_2. It implies that the effect of the fixed boundary for ILMs depends on the nonlinear coupling coefficient. This dependency is discussed in more detail with the stability of ILMs in Sec. III C.

C. Stability of coexisting ILMs

Eigenvalues of ST4 and P4-5 at $\beta_2=0.001$ are shown in Fig. 4. All of the eigenvalues for ST4 are on a unit circle, as shown Fig. 4(a). Then ST4 is not determined to be unstable. A solution stays around ST4 for a long period when an initial condition of the solution is chosen near ST4. Thus, the stability of ST4 is called "marginally stable."[3] In fact, if Eq. (1) has some damping terms, then the absolute values of all eigenvalues are less than unity. Figure 4(b) shows eigenvalues of P4-5. One of the eigenvalues is outside the unit circle.

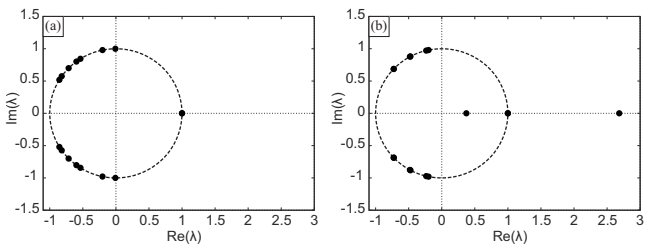

FIG. 4. Eigenvalues of the linearized map $\mathcal{DP}(\mathbf{x}^*)$ at $\beta_2=0.001$: (a) ST4 and (b) P4-5. The circle drawn by dashed curve indicates unit circle in the complex plane.

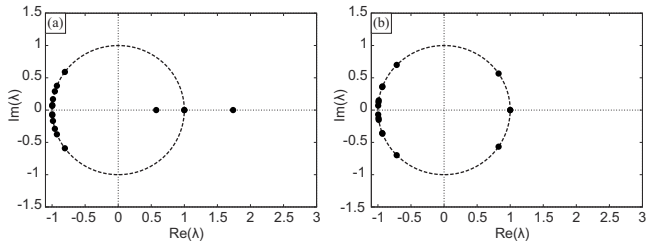

FIG. 5. Eigenvalues of the linearized map $\mathcal{DP}(\mathbf{x}^*)$ at $\beta_2=0.001$: (a) ST4 and (b) P4-5.

Then P4-5 is unstable. All coexisting P modes are unstable and ST modes are stable at $\beta_2=0.001$. However the stability of coexisting ILMs are flipped at $\beta_2=0.01$. ST4 at $\beta_2=0.01$ is unstable, as shown in Fig. 5(a). Then P4-5 is stable. It implies that the stability change occurs between $\beta_2=0.001$ and 0.01.

Figure 6 shows the stability and the locus of each coexisting ILM with respect to the nonlinear coupling coefficient, β_2. The locus of ILM is obtained by

$$X_{\mathrm{ILM}}=\frac{\Sigma_{n=1}^{8} n\times|u_n|}{\Sigma_{n=1}^{8}|u_n|}, \tag{4}$$

where $|u_n|$ is the absolute value of nth oscillator's displacement on the hyper surface Σ_4. The set of stable ILMs is represented by the solid curve. The dashed curves correspond to unstable ILMs. The figure clearly shows that the stability of coexisting ILMs is flipped with the nonlinear coupling coefficient, β_2. In particular, ILMs standing around the center of array almost simultaneously gain or lose stability at $\beta_2\simeq 0.005\,45$.[18] On the other hand, ST1 and P1-2 coincide at $\beta_2\simeq 0.002\,38$ and disappear with increment of β_2. The P1-2 appears again with ST2 at $\beta_2\simeq 0.007\,16$. Such appearance and disappearance are classified as saddle-node bifurcation.[18]

Figure 6 shows that a bifurcation point tends to depart from $\beta_2\simeq 0.005\,45$ as the locus of ILM approaches the end of array. This parameter gap seems to be affected by the fixed ends. In fact, the gap is vanished in the ringed array.[18] Since the fixed end can be thought as an impurity, the parameter gap can also be obtained by adding an impurity. Thus, Fig. 6 also shows the magnitude of the effect of an impurity with respect to the coupling nonlinearity. The influence of an impurity has a peak near $\beta_2\simeq 0.005\,45$ that corresponds to the stability change in ILMs standing near the center of array.

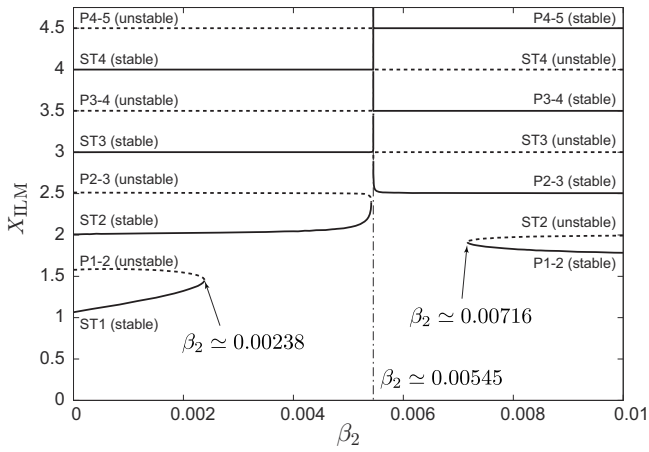

FIG. 6. Locus and stability of coexisting ILMs. The solid curve corresponds to stable ILMs. Unstable ILMs are represented by the dashed curve.

IV. TRAVELING ILM AND PHASE STRUCTURE

A. Relationship between traveling ILM and invariant manifold

Perturbation against an unstable ILM generates a traveling ILM. Trajectory of the traveling ILM is determined by phase structure around the unstable ILM.[21] The phase structure is characterized by invariant manifolds of the unstable ILM. Each unstable ILM in coexisting ILMs has only one eigenvalue outside the unit circle. Then the unstable manifold of each unstable ILM is one-dimensional. In addition, the stable manifold is also one dimensional since Eq. (1) can be reversed with respect to time.

We applied a projection $\mathcal{G}:\Sigma_p\to\mathbb{C}$ for drawing invariant manifolds, where $\mathbb{C}$ means the set of all complex numbers. The projection is defined as[27]

$$h_k=\mathcal{G}(\mathbf{x}_k)=\sum_{n=0}^{N}\left\{\frac{1}{2}\dot{u}_n^2 e^{i(2\pi/N)n}+U_{\mathrm{On}}(u_n)e^{i(2\pi/N)n}+U_{\mathrm{In}}(u_n-u_{n-1})e^{i(2\pi/N)(n+(1/2))}\right\}, \tag{5}$$

where $N=9$. The fixed boundaries are denoted by u_0 and u_9. The values of u_0 and u_9 are kept at zero. On-site and intersite potentials of the nth oscillator are represented by U_{On} and U_{In}, respectively. The on-site and the intersite potentials are given by

$$U_{\mathrm{On}}(u_n)=\frac{\alpha_1}{2}u_n^2+\frac{\beta_1}{4}u_n^4,$$
$$U_{\mathrm{In}}(u_n-u_{n-1})=\frac{\alpha_2}{2}(u_n-u_{n-1})^2+\frac{\beta_2}{4}(u_n-u_{n-1})^4. \tag{6}$$

The locus of an ILM is given by $\theta_k=\arg h_k$. The velocity of an traveling ILM can be estimated from the difference between θ_k and θ_{k+1}.[27]

The structure of unstable manifolds is schematically drawn by projection. Figure 7(a) shows the structure at $\beta_2=0.001$. In Fig. 7(a), stable and unstable ILMs are represented by open circles and squares, respectively. Unstable manifolds are drawn by solid curves. The unstable manifold of P3-4 has a cyclic structure, which is centered between P3-4 and ST4 in Fig. 7(a). The structure implies that a traveling ILM initially excited near P3-4 wanders between P3-4 and ST4. In Fig. 7(b), the behavior of the traveling ILM is shown with energy distribution given by Eq. (6). The dark region corresponds to high energy state. At first, the energy is mainly distributed on the third and fourth sites and between them. The locus of the energy distribution is at 3.5. In other words, the traveling ILM stays near P3-4. The traveling ILM suddenly moves to ST4 at $t\simeq 50$. The energy concentrates on

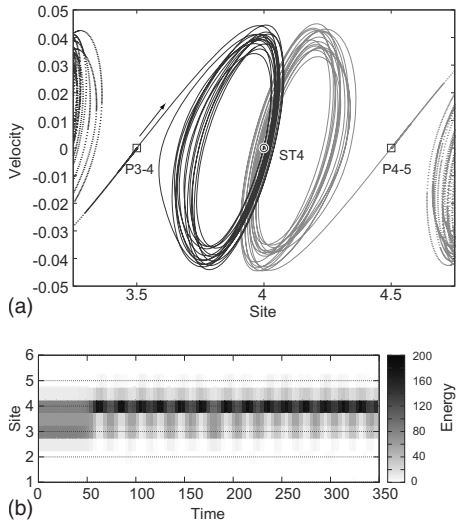

FIG. 7. (a) Unstable manifold of P3-4 and P4-5. Coexisting ILMs are represented by circles and squares. The arrow in the upper panel implies the direction of a perturbation against P3-4. The dots lying on the upper left are caused by definition of the hyper plane Σ_4. (b) Temporal development of a traveling ILM. Darkness corresponds to the energy.

the third oscillator at $t=60$. Then the traveling ILM immediately returns to P3-4. Finally the traveling ILM reciprocally moves for a long period. Figures 7(a) and 7(b) show that the behavior of the traveling ILM is predictable by the structure of unstable manifolds in the phase space.

Unstable manifolds of unstable ST modes at $\beta_2=0.01$ are shown in Fig. 8(a). The unstable manifolds have cyclic structures as well as the unstable manifolds of P modes at $\beta_2=0.001$. However, the cyclic structures of the unstable manifolds of ST modes are centered at a stable P mode. The unstable manifold of ST4 is located nearby ST5 and vice versa. Thus, a traveling ILM will move from the vicinity of ST4 toward ST5 if the traveling ILM is excited near the ST4. The behavior of the traveling ILM is shown in Fig. 8(b). The traveling ILM that was initially at $n=4$ begins to move at $t\simeq 50$. Finally the traveling ILM reciprocally moves between

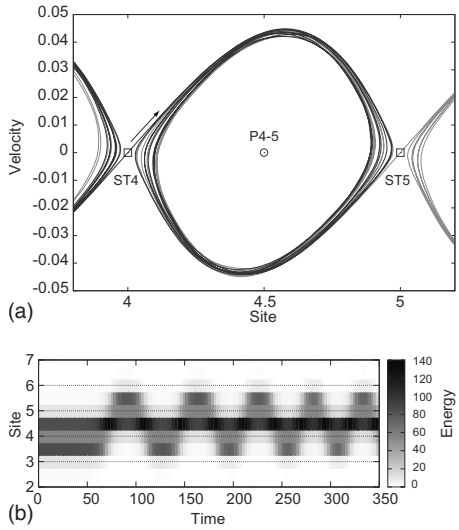

FIG. 8. (a) Unstable manifold of ST3, ST4, and ST5. (b) Temporal development of a traveling ILM.

ST4 and ST5. The reciprocal behavior corresponds to the structure of the unstable manifolds. In addition, the traveling ILM maintains its localized energy distribution, while it wanders in the array. Therefore, the structure of unstable manifolds implies the behavior of a traveling ILM, which is generated near an unstable ILM.

B. Invariant manifold and nonlinear coupling coefficient

The structure of unstable manifolds in phase space also depends on the nonlinear coupling coefficient because the stability of coexisting ILMs is flipped by varying β_2. Figure 8 shows the structure of unstable manifolds at $\beta_2=0.003$, 0.005, and 0.006. The stability change occurs between $\beta_2=0.005$ and 0.006. Unstable manifolds of P modes at $\beta_2=0.003$ have cyclic structures. The phase structure shown in Fig. 8(a) asymptotically changes to Fig. 8(b) with increasing β_2. Figure 8(b) shows a simple structure similar to the phase space of a pendulum system. The inset in Fig. 8(b) shows the structure around P3-4. There is no hetero- or homoclinic connection. The phase structure at $\beta_2=0.006$ is also a simple structure. In Fig. 8(c), the unstable manifold of ST4 reaches both the vicinity of ST5 and ST4. If β_2 increases from 0.006 to 0.01, the structure changes to Fig. 8(a). Therefore, the structure of unstable manifolds in phase space is changed with its cyclic structures maintained with respect to the nonlinear coupling coefficient. However, the structure is drastically changed when the stability change occurs. In Sec. V, the drastic change is applied to a manipulation of a traveling ILM.

V. CAPTURE AND RELEASE

The behavior of a traveling ILM is determined by the structure of unstable manifolds in phase space. Thus, the traveling ILM can be manipulated by changing the phase structure. In the microcantilever array, the nonlinear coupling coefficient flips the stability of coexisting ILMs and changes the phase structure. In this section, *capture* and *release* of a traveling ILM is numerically discussed.

We assume that a traveling ILM is initially excited near a coexisting ILM, which is stable. The traveling ILM stays around the stable ILM. If the stability change is caused by rapid shift of the nonlinear coupling coefficient, the traveling ILM begins to move along the unstable manifold of the destabilized ILM. That is to say, the traveling ILM is released. The released ILM will wander in the array. The wandering ILM can be captured by the stability change if the wandering ILM approaches to the vicinity of an unstable ILM. The captured ILM stays around the stabilized ILM.

Capture and release of a traveling ILM is numerically shown in Fig. 9(a). An ILM initially stands at P3-4. In the initial state, the nonlinear coupling coefficient is set at $\beta_2=0.006$. Thus, the P3-4 is stable. The nonlinear coupling coefficient is discontinuously changed from 0.006 to 0.005 at $k=69$, where k denotes the map number corresponding to the time evolution. As a result, the first stability change is caused. The ILM is released. The released ILM leaves from the destabilized P3-4 at $k\simeq 110$. Then it approaches to the

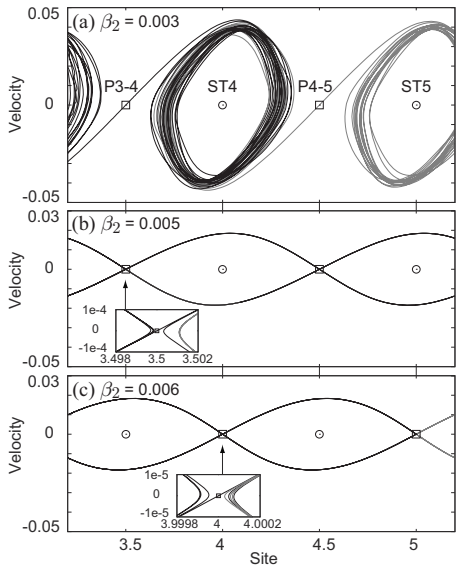

FIG. 9. Schematic relationship between coexisting ILMs and unstable manifolds for (a) β_2=0.003, (b) 0.005, and (c) 0.006. The structure of the vicinity of an unstable ILM is shown in the insets. Unstable manifolds are located very close to the unstable ILM. There is no homo- or heteroclinic connection.

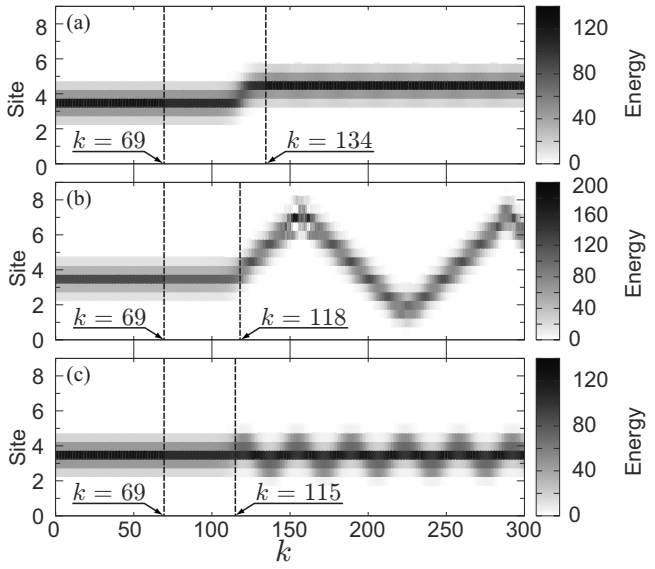

FIG. 10. Capture and release of traveling ILM. A stable ILM is initially excited. The stability of coexisting ILMs is changed at k=69, where k depicts the number of the map and corresponds to the time development. The nonlinear coupling coefficient is instantaneously changed here. The stability is flipped again at (a) k=134, (b) 118, and (c) 115.

vicinity of P4-5 because the unstable manifold of P3-4 reaches near the P4-5 [see Fig. 8(b)]. After the released ILM reaches the P4-5, β_2 is set at 0.006 again at k=134. The P4-5 gains stability by the second stability change. The released ILM is captured around the stabilized P4-5. Consequently, the ILM travels from P3-4 to P4-5.

However, the released ILM is not captured if the second stability change is caused at k=118, as shown in Fig. 9(b). The ILM travels in the whole of array. The direction of the traveling ILM is turned by the end of array. On the other hand, Fig. 9(c) shows that the released ILM is captured around the ILM where the traveling ILM initially stands. The second stability change is caused at k=115. The traveling ILM reciprocally moves around P3-4. The difference in the behavior is due to the phase structures. A released ILM travels along unstable manifolds from unstable P3-4, as shown in Fig. 10(a). After the second stability change, the phase structure is drastically changed. Figure 10(b) shows the phase structure and trajectories of traveling ILMs after the second stability change. For the trajectory corresponding to Fig. 9(b), the traveling ILM is located outside all cyclic structures of unstable manifolds. On the other hand, the traveling ILM is inside the cyclic structure for the trajectory in Figs. 9(a) and 9(c). It implies that if a traveling ILM released by the first stability change is inside the cyclic structure when the second stability change occurs, the traveling ILM is captured around a stabilized ILM. In addition, a traveling ILM wandering the whole of array is generated if the traveling ILM is located outside all cyclic structures (see Fig. 11).

The manipulation using the stability change requires that the nonlinear coupling coefficient β_2 of Eq. (1) is adjustable. The nonlinear on-site coefficient β_1 can also flip the stability because the ratio β_2/β_1 determines the stability of coexisting ILMs.[18] It has been reported that an on-site nonlinearity can be adjustable by applying a static electric field to a microcantilever array.[17] The electric field is applied between each cantilever and a substrate facing the array, and an electric force is thus induced in each cantilever. The on-site potential is modified as $U_{On}(u_n)=\alpha_1 u_n^2/2+\beta_1 u_n^4/4-\delta_1 V^2/(d_0'+u_n)$,[17,28] where d_0' and V depict a nondimensionalized distance and the voltage between the cantilever array and the substrate, respectively. The relative magnitude of the static electric potential is determined by a coefficient δ_1 which depends on the size of cantilever. According to Maclaurin's expansion, an applied electric field changes the on-site nonlinear coefficient as $\beta_1'=\beta_1-4\delta_1 V^2/d_0'^5$. Therefore the on-site nonlinearity can be varied as a function of the voltage. If a microcan-

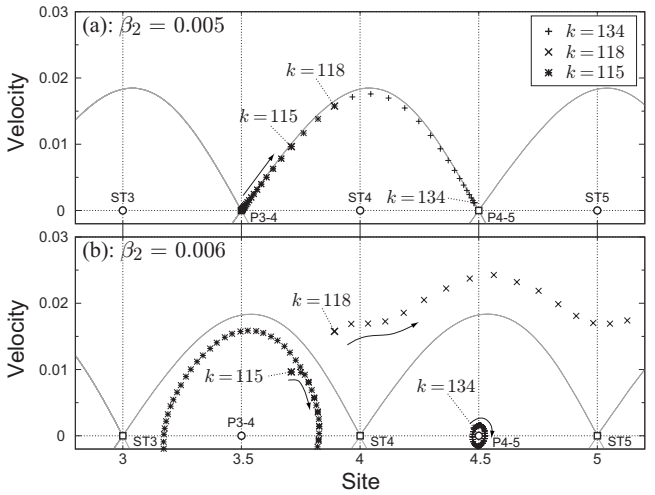

FIG. 11. Trajectories of traveling ILMs and unstable manifolds of unstable ILMs. The trajectories are projected by $\mathcal{G}$. Open circles and boxes correspond to coexisting ILMs. Gray curves represent unstable manifolds of unstable ILMs. The trajectories are drawn by sequences of points. (a) Trajectories during the first and the second stability changes, and (b) trajectories after the second stability change.

tilever array is fabricated to have the stable ST modes, the manipulation is possible because an applied voltage decreases the nonlinear on-site coefficient.

In addition, a macromechanical cantilever array with tunable on-site nonlinearity is also proposed to study the manipulations of ILM.[29] The dynamics of the macrocantilever array is similar to the coupled oscillators discussed in this paper. On-site potential of each cantilever is adjusted by an static magnetic field caused by an electromagnet facing to the tip of the cantilever. Because each cantilever has a permanent magnet at the free end, the magnetic field causes a nonlinearity in the on-site potential. The nonlinearity is easily varied by adjusting the current flowing in the electromagnets. Consequently, the manipulation method using parameter adjustment can be confirmed experimentally for both micro- and macrocantilever arrays.

VI. CONCLUSION

In this paper, it has been shown how a traveling ILM behaves in the phase space. Unstable manifolds of unstable coexisting ILMs strongly affect the behavior of traveling ILM. That is, it is suggested that the structure of unstable manifolds in the phase space governs the traveling ILM.

On the basis of the fact that the global phase structure is changed by a nonlinear coefficient in the coupled oscillators, we have proposed a new method to manipulate ILM. Since the equation of motion of the coupled oscillators is generalized by nondimensionalization, the results in this paper can be applied to various systems without loss of generality. In addition, the possibility to realize the manipulation in experiments is discussed for micro- and macrocantilever arrays. In micrometer scale, a static electric field can vary a nonlinear on-site coefficient as a function of the voltage between the cantilever array and the substrate. On the other hand, a static magnetic field can be used to adjust the nonlinear on-site coefficient in macroscale. Therefore the manipulation using stability change can be possibly applied to experimental systems.

ACKNOWLEDGMENTS

The authors would like to thank Professor Masayuki Sato, Kanazawa University, Japan, for his helpful comments and discussions. One of the authors (M.K.) would like to thank Dr. Kazuyuki Yoshimura, NTT corporation, Japan, for fruitful discussions regarding the stability of ILMs. This research was partially supported by the Ministry of Education, Culture, Sports, Science and Technology in Japan, The 21st Century COE Program No. 14213201, and the Global COE program.

[1] A. J. Sievers and S. Takeno, Phys. Rev. Lett. **61**, 970 (1988).
[2] E. Fermi, J. Pasta, and S. Ulam, *The Collected Papers of Enrico Fermi* (University of Chicago Press, Chicago, 1955), Vol. 2, pp. 978–988.
[3] S. Flach and C. R. Willis, Phys. Rep. **295**, 181 (1998).
[4] D. K. Campbell, S. Flach, and Y. S. Kivshar, Phys. Today **57**(1), 43 (2004).
[5] E. Trías, J. J. Mazo, and T. P. Orlando, Phys. Rev. Lett. **84**, 741 (2000).
[6] P. Binder, D. Abraimov, A. V. Ustinov, S. Flach, and Y. Zolotaryuk, Phys. Rev. Lett. **84**, 745 (2000).
[7] H. S. Eisenberg, Y. Silberberg, R. Morandotti, A. R. Boyd, and J. S. Aitchison, Phys. Rev. Lett. **81**, 3383 (1998).
[8] R. Morandotti, U. Peschel, J. S. Aitchison, H. S. Eisenberg, and Y. Silberberg, Phys. Rev. Lett. **83**, 2726 (1999).
[9] J. W. Fleischer, M. Segev, N. K. Efremidis, and D. N. Christodoulides, Nature (London) **422**, 147 (2003).
[10] M. Sato, B. E. Hubbard, A. J. Sievers, B. Ilic, D. A. Czaplewski, and H. G. Craighead, Phys. Rev. Lett. **90**, 044102 (2003).
[11] B. I. Swanson, J. A. Brozik, S. P. Love, G. F. Strouse, A. P. Shreve, A. R. Bishop, W.-Z. Wang, and M. I. Salkola, Phys. Rev. Lett. **82**, 3288 (1999).
[12] K. Kisoda, N. Kimura, H. Harima, K. Takenouchi, and M. Nakajima, J. Lumin. **94–95**, 743 (2001).
[13] M. Sato and A. J. Sievers, Nature (London) **432**, 486 (2004).
[14] M. Sato, S. Yasui, M. Kimura, T. Hikihara, and A. J. Sievers, Europhys. Lett. **80**, 30002 (2007).
[15] M. Sato, B. E. Hubbard, L. Q. English, A. J. Sievers, B. Ilic, D. A. Czaplewski, and H. G. Craighead, Chaos **13**, 702 (2003).
[16] M. Sato, B. E. Hubbard, A. J. Sievers, B. Ilic, and H. G. Craighead, Europhys. Lett. **66**, 318 (2004).
[17] M. Sato, B. E. Hubbard, and A. J. Sievers, Rev. Mod. Phys. **78**, 137 (2006).
[18] M. Kimura and T. Hikihara, Phys. Lett. A **372**, 4592 (2008).
[19] T. Hikihara, Y. Okamoto, and Y. Ueda, Chaos **7**, 810 (1997).
[20] T. Hikihara, K. Torii, and Y. Ueda, Phys. Lett. A **281**, 155 (2001).
[21] T. Hikihara, K. Torii, and Y. Ueda, Int. J. Bifurcation Chaos Appl. Sci. Eng. **11**, 999 (2001).
[22] M. R. M. Crespo da Silva and C. C. Glynn, J. Struct. Mech. **6**, 437 (1978).
[23] M. R. M. Crespo da Silva, Int. J. Solids Struct. **24**, 1225 (1988).
[24] P. Malatkar and A. H. Nayfeh, Nonlinear Dyn. **31**, 225 (2003).
[25] W. H. Press, S. A. Teukolsky, W. T. Vetterling, and B. P. Flannery, *Numerical Recipes in C*, 2nd ed. (Cambridge University Press, New York, 1992).
[26] L. M. Marín and S. Aubry, Nonlinearity **9**, 1501 (1996).
[27] P. A. Houle, Phys. Rev. E **56**, 3657 (1997).
[28] M. I. Younis and A. H. Nayfeh, Nonlinear Dyn. **31**, 91 (2003).
[29] M. Kimura and T. Hikihara, Phys. Lett. A **373**, 1257 (2009).